Folate-targeted liposomal nitrooxy-doxorubicin: An effective tool against P-glycoprotein-positive and folate receptor-positive tumors

(Article begins on next page)

27 July 2024

Folate-targeted liposomal nitrooxy-doxorubicin: an effective tool against P-glycoprotein-positive and folate receptor-positive tumors

Elena Gazzano [a,§], Barbara Rolando [b,§], Konstantin Chegaev [b], Iris C. Salaroglio [a], Joanna Kopecka [a], Isabella Pedrini [b], Simona Saponara [c], Matteo Sorge [d], Ilaria Buondonno [a], Barbara Stella [b], Alessandro Marengo [b], Massimo Valoti [c], Mara Brancaccio [d], Roberta Fruttero [b], Alberto Gasco [b,§], Silvia Arpicco [b,§,*], Chiara Riganti [a,§,*]

[a] Department of Oncology, University of Torino, via Santena 5/bis, 10126, Torino, Italy

[b] Department of Drug Science and Technology, University of Torino, via Pietro Giuria 9, 10125 Torino, Italy

[c] Department of Life Sciences, University of Siena, via Aldo Moro 2, 53100 Siena, Italy

[d] Department of Molecular Biotechnology and Health Sciences, University of Torino, via Nizza 52, 10126, Torino, Italy

[§] Equal contribution

Corresponding authors: Dr. Silvia Arpicco, Department of Drug Science and Technology, University of Torino, via Pietro Giuria 9, 10125 Torino, Italy; phone: +39116706668; fax: +39116706663; email: silvia.arpicco@unito.it; Dr. Chiara Riganti, Department of Oncology, University of Torino, via Santena 5/bis, 10126 Torino, Italy; phone: +39116705857; fax: +39116705845; email: chiara.riganti@unito.it

Abstract

Drug efflux transporters, in particular P-glycoprotein (Pgp), limit the success of chemotherapy. We previously found that synthetic doxorubicin conjugated with nitric oxide (NO)-releasing group overcomes resistance by inducing a NO-mediated inhibition of Pgp. Here we produced the first liposomal formulations of this nitrooxy-doxorubicin decorated with folic acid (FA), termed LNDF, in order to improve their active targeting against Pgp-expressing tumors. Folate was inserted onto liposomes surface using two different methods and the formulations were compared with respect to their technological features and *in vitro* behavior. By analyzing human and murine breast cancer cells with different expression of FA receptor (FAR) and Pgp, we demonstrated that LNDF are internalized in a FAR-dependent manner and achieve maximal anti-tumor efficacy against FAR-positive/Pgp-positive cells. Upon uptake of LNDF, nitrooxy-doxorubicin was delivered within nucleus, where it induced cell cycle arrest and DNA damages, and mitochondria, where it impaired the mitochondrial energy metabolism and triggered mitochondria-dependent apoptosis. LNDF reduced the growth of FAR-positive/Pgp-positive tumors and prevented tumor formation in mice, whereas doxorubicin and Caelyx® failed. LNDF cardiotoxicity was comparable to Caelyx®. The sensitivity to LNDF was maintained in tumors exposed to repeated cycles of the drug and in cells derived from the exposed tumors, excluding the onset of secondary resistance.

By combining an innovative multitarget cargo drug, conceived to achieve high efficacy against Pgp-expressing cells, and appropriate strategies of liposome formulation and decoration, we produced a therapeutic tool that may represent a significant advancement in the treatment of FAR-positive/Pgp-positive tumors.

Keyword: liposomes; doxorubicin; folic acid; P-glycoprotein; chemoresistance; breast cancer

1 Introduction

Multidrug resistance (MDR) is a multiple resistance towards different chemotherapeutic drugs, unrelated for structures and pharmacodynamic properties. One of the main mechanisms of MDR is the high expression on cell surface of ATP binding cassette (ABC) transporters, such as P-glycoprotein (Pgp), MDR-related proteins (MRPs), breast cancer resistance protein (BCRP), lung resistance protein (LRP). For the broad spectrum of substrates, including anthracyclines like doxorubicin (Dox), taxanes, vinca alkaloids, epipodophyllotoxins, topotecan, methotrexate, and targeted-therapies such as imatinib, dasatinib, lapatinib, gefitinib, sorafenib, and erlotinib, Pgp is one of the main determinant of MDR [1, 2].

Natural and synthetic inhibitors of ABC transporters have been tested to reverse MDR phenotype: although successful *in vitro*, they often failed *in vivo* for the low specificity, the side-effects induced and the drug-drug interactions that produced unexpected toxicity [3]. Recently, small molecules endorsed with specific cytotoxicity against ABC transporter-expressing cells have been widely studied as a new approach to overcome MDR. However, the poor mechanistic knowledge at the basis of their selective cytotoxicity for MDR cells, an event known as "collateral sensitivity" [4], has limited the application of these agents to *in vitro* models. Gene-silencing of ABC transporters, co-delivery of ABC-transporter silencers and chemotherapeutic drug [5], inhibition of transcription factors that up-regulate these proteins [6] or of surface proteins adjuvanting ABC transporters activity [7] have been also experimented *in vitro* and in preclinical models, but the translation potential of these approaches to oncological patients is far.

We recently developed multi-target synthetic derivatives of Dox, conjugated with substructures releasing nitric oxide (NO); by nitrating critical tyrosines on ABC transporters, NO impairs the catalytic activity of the pumps, allowing the increased intracellular retention and cytotoxicity of Dox [8]. Besides inhibiting their own efflux [9,10], some of these NO-releasing doxorubicins - like the

nitrooxy-Dox derivative (ND) - revealed pharmacodynamic properties completely different from parental Dox [11,12].

Liposomal formulations of ND (LND) were effective *in vitro* against human breast and ovary cancer drug-resistant cells, showing a superior efficacy to Caelyx® [13], the Dox liposomal formulation used in patients bearing these type of tumors [14].

To further refine the tumor specificity and efficacy of LND, in this work we produced and validated LND formulations decorated with folic acid (FA), termed LNDF. Since FA is not-immunogenic and binds with high specificity to the FA receptor (FAR), a protein overexpressed in many tumor cells respect to not transformed cells [15], it is an effective small molecule for active targeting of liposomes and nanoparticles. To validate the efficacy of our formulations, we focused on drug-resistant Pgp-positive breast tumors, that include up to 56% tumors positive for FAR [16]. A part the reduced cardiotoxicity, Caelyx® did not offer a significant advance over Dox in the treatment of breast tumors [14], leaving the field open to the research of more effective anthracycline-based treatments. This is of particular importance for triple negative breast cancers, where anthracycline- or taxane-based monotherapy regimes are the first-line treatment [17], but the rate of success of pharmacological therapy is lower compared to other breast cancer types [18].

The aim of the present work was to produce, characterize, and validate LNDF as an effective and safe tool against Pgp-positive chemoresisstant breast cancers.

Materials and methods

Chemicals. All the phospholipids were provided by Avanti Polar-Lipids distributed by Spectra 2000 (Rome, Italy). Folate-polyethylene glycol-distearoylphosphatidylethanolamine (FA-PEG-DSPE; PEG mean molecular weight, 3400 Da) was obtained from NANOCS distributed by DBA Italia (Segrate, Milano, Italy). Cholesterol, Dox and all the other chemicals were obtained from Sigma Chemical Co.

(St. Louis Mo). All the solvents used were of analytical grade, purchased from Carlo Erba Reagenti (Milan, Italy). Fetal bovine serum (FBS), fetal calf serum (FCS) and culture medium were supplied by Invitrogen Life Technologies (Carlsbad, CA); plasticware for cell cultures was from Falcon (Bectison Dickinson, Franklin Lakes, NJ). Electrophoresis reagents were obtained from Bio-Rad Laboratories (Hercules, CA); the protein content of cell monolayers and lysates was assessed with the BCA kit from Sigma Chemical Co. The synthesis of nitrooxy-doxorubicin was performed as described previously [9].

Preparation of liposomes. Liposomes containing ND (LND) were prepared as previously described [13]. Folate-targeted liposomes (LNDFm and LNDFpi) were prepared with two different methods. LNDFm were prepared by adding the FA-PEG-DSPE conjugate to the other phospholipids during lipid film preparation. Briefly, chloroform or methanol solution of 1,2-distearoyl-*sn*-glycero-3-phosphocholine (DSPC), cholesterol (Chol), 1,2-distearoyl-*sn*-glycero-3-phosphoethanolamine-N-[amino(polyethylene glycol)-2000] (mPEG-DSPE, ammonium salt) and FA-PEG-DSPE, at a molar ratio of 75.7:18.9:2.7:2.7 and containing ND (11% ratio mol drug/mol lipid) were evaporated and the resulting lipid film was dried under vacuum overnight. The thin film was then hydrated with a 20 mM 4-(2-hydroxyethyl)piperazine-1-ethanesulforic acid (HEPES) buffer (pH 7.4) and the suspension was vortex mixed for 10 min and bath sonicated. The formulations were then sequentially extruded (Extruder, Lipex, Vancouver, Canada) through 400 and then 200 nm polycarbonate membrane (Costar, Corning Incorporated, NY) at a set temperature of 5°C above the phase transition temperature of the lipid mixture. Liposomal preparations were purified from non-encapsulated ND through chromatography on Sepharose CL-4B columns, eluting with HEPES buffer at room temperature.

LNDFpi were prepared by adding the FA-PEG-DSPE conjugate by post insertion method [19] into pre-formed liposomes composed by DSPC/Chol/mPEG-DSPE in a molar ratio of 75.7:18.9:5.4 and ND (11% ratio mol drug/mol lipid) prepared as previously described. Liposomes were incubated with a concentrated micellar FA-PEG-DSPE conjugate solution at 60°C for 2 h, at a ligand molar ratio of

3.2% relative to total phospholipids. Then, the mixture was cooled and liposomes were purified from excess of FA-PEG-DSPE conjugate and ND through chromatography on Sepharose CL-4B column, eluting with HEPES buffer.

Liposome characterization. The mean particle size and polydispersity index of the liposomes were determined at 20°C by Quasi-elastic light scattering (QELS) using a nanosizer Coulter® N4MD (Coulter Electronics, Inc., Hialeah, FL). The selected angle was 90° and the measurement was taken after dilution of the liposome suspensions in MilliQ® water. Each measurement was carried out in triplicate. The surface charge of liposomes was evaluated by zeta potential measurements after dilution of the suspensions in 10 mM KCl using a Zetasizer (Zeta Potential Analyzer Ver. 2.17, Brookhaven Inst. Corp., Holtsville, NY). Phospholipid phosphorous was assessed in each liposome preparation by phosphate assay after destruction with perchloric acid [20].

The amount of ND incorporated in liposomes was determined by reverse phase (RP)-HPLC as previously reported [13].

The total amount of folate and the number of folate molecules per liposome were determined spectroscopically at 285 nm by comparison to a standard curve of FA and the known lipid concentration [21].

The colloidal stability of the suspensions was evaluated by measuring the mean size of the formulations over a storage period of 28 days at 4 °C; the stability was also tested in HEPES buffer and FCS at 37 °C for 48 h.

To evaluate ND release in FCS the formulations were diluted 1:2.5 with FCS and incubated at 37°C for various periods of time; drug leakage was determined submitting 200 µL of liposomes to purification through chromatography on Sepharose CL-4B columns, eluting with HEPES buffer. Then, the drug and lipid content was measured in the collected liposomal fractions and compared with initial values. For comparison, a drug leakage study was also performed in HEPES buffer at 37°C.

Cell lines. Human non transformed breast epithelial MCF10A cells, human breast cancer MCF7, SKBR3, T74D, MDA-MB-231 cells, human osteosarcoma U-2OS cells, murine mammary cancer JC cells were purchased from ATCC (Manassas, VA). Murine mammary cancer TUBO cells were a kind gift of Prof. Federica Cavallo, Department of Molecular Biotechnology and Health Sciences, University of Turin, Italy. Cells were maintained in mediums supplemented with 10% v/v fetal bovine serum, 1% v/v penicillin-streptomycin, 1% v/v L-glutamine.

Immunoblotting. Cells were lysed in MLB buffer (125 mM Tris-HCl, 750 mM NaCl, 1% v/v NP40, 10% v/v glycerol, 50 mM $MgCl_2$, 5 mM EDTA, 25 mM NaF, 1 mM $NaVO_4$, 10 μg/mL leupeptin, 10 μg/mL pepstatin, 10 μg/mL aprotinin, 1 mM phenylmethylsulfonyl fluoride, pH 7.5), sonicated and centrifuged at 13,000 x g for 10 min at 4°C. 20 μg of proteins from cell lysates or tumor homogenates were subjected to Western blotting and probed with the following antibodies: anti-FAR antibody (Abcam, Cambridge, UK); anti-Pgp (BD Biosciences, San Josè, CA), anti-MRP1 (Abcam, Cambridge, UK), anti-tubulin (Santa Cruz Biotechnology Inc., Santa Cruz, CA). The proteins were detected by enhanced chemiluminescence (Bio-Rad Laboratories).

Flow cytometry. Cells were washed with PBS, detached with Cell Dissociation Solution (Sigma) and re-suspended in culture medium containing 5 % v/v FBS. Samples were washed with 0.25% w/v PBS-bovine serum albumin (BSA), incubated with the primary antibody for anti-FAR for 45 min at 4°C, then washed twice and incubated with the secondary fluorescein isothiocyanate-conjugated antibody for 30 min at 4°C. After washing and fixation in paraformaldehyde 2 w/v %, the surface amount of FAR was detected on 100,000 cells by a FACSCalibur system (Becton Dickinson), using the Cell Quest software (Becton Dickinson). Control experiments included incubation of cells with non-immune isotypic antibody, followed by secondary antibody.

Cellular uptake of doxorubicins. Cells were incubated with Dox, ND or respective formulations for 0, 1, 3, 6, and 24 h. The amount of compounds in cell lysates was measured spectrofluorimetrically, as

described in [8] using a Synergy HT Multi-Detection Microplate Reader (Bio-Tek Instruments, Winooski, VT). Excitation and emission wavelengths were 475 and 553 nm, respectively. A blank was prepared in the absence of cells for each set of experiments, and its fluorescence was subtracted from that measured in the presence of cells. In competition assays, cells were incubated 6 h with 5 μM folate-targeted liposomes, in the presence of an excess of free FA (50 μM) or a saturating amount of anti-FAR antibody (100 μg/mL). The amount of intracellular compounds was measured as reported above; fluorescence was converted to nmol Dox/mg cell or tissue proteins using a calibration curve prepared previously. The amount of doxorubicins in nuclear and mitochondrial extracts (see below) was measured by HPLC, as reported in [11]. Results were expressed as nmoles doxorubicins/mg cell proteins.

Nitrite production. Nitrite production was measured by adding 0.15 mL of cell culture medium to 0.15 mL of Griess reagent in a 96-well plate, and after a 10 min incubation at 37°C in the dark, the absorbance was detected at 540 nm with a Packard EL340 microplate reader (Bio-Tek Instruments). A blank was prepared for each experiment in the absence of cells, and its absorbance was subtracted from the one obtained in the presence of cells. Nitrite concentration was expressed as nmoles/mg cell proteins.

Extracellular lactate dehydrogenase (LDH) activity. To verify the cytotoxic effect of compounds, the extracellular medium was centrifuged at $12,000 \times g$ for 15 min to pellet cellular debris, whereas cells were washed with fresh medium, detached with trypsin/EDTA, re-suspended in 0.2 mL of 82.3 mM triethanolamine phosphate-HCl (pH 7.6) and sonicated on ice with two 10 s bursts. LDH activity was measured in the extracellular medium and in the cell lysate, as reported [8]. The reaction was followed for 6 min, measuring absorbance at 340 nm with Packard EL340 microplate reader (Bio-Tek Instruments) and was linear throughout the time of measurement. Both intracellular and extracellular

1 enzyme activity was expressed in μmoles NADH oxidized/min/dish, then extracellular LDH activity

2 was calculated as percentage of the total LDH activity in the dish.

3 **Cell viability.** Cell viability was measured by the neutral red staining method, as previously reported

4 [22]. The absorbance at 540 nm was read using a Synergy HT Multi-Detection Microplate Reader (Bio-

5 Tek Instruments). The absorbance of untreated cells was considered as 100% viability; the results were

6 expressed as percentage of viable cells *versus* untreated cells.

7 **Fluorescence and confocal microscope analysis.** For fluorescence microscopy analysis, 0.5×10^5 cells

8 were grown on sterile glass coverslips, then rinsed with PBS, fixed with 4% w/v paraformaldehyde for

9 15 min, washed three times with PBS and incubated with 4′,6-diamidino-2-phenylindole

10 dihydrochloride (DAPI, diluted 1: 20000) for 3 min at room temperature in the dark. Fluorescently

11 labelled cells were washed three times with PBS and once with water, then the slides were mounted

12 with 4 μl of Gel Mount Aqueous Mounting and examined using a Leica DC100 microscope (Leica

13 Microsystems, Wetzlar, Germany) with a 63 x oil immersion objective and 10 x ocular lens. In

14 confocal microscopy analysis for compounds intracellular localization, cells were previously

15 transfected with expression vectors encoding for the GFP-fused-leader sequence of E1-α-pyruvate

16 dehydrogenase to label mitochondria for 18 h (Cell Light BacMan 2.0, Invitrogen), then incubated for 6

17 h with the compounds and prepared as reported above. Image acquisition was performed with a Leica

18 TCS SP2 AOBS confocal laser-scanning microscope with a 63 x oil immersion objective and 10 x

19 ocular lens. For each experimental point, a minimum of 5 microscopic fields were examined. Imaging

20 quantification was performed with ImageJ software (*https://imagej.nih.gov/i*). Fluorescence intensity in

21 cells treated with Dox was set as 1 unit. Results were expressed as relative fluorescence units (RFU).

22 **Cytosol-nucleus separation.** Cells were mechanically scraped in PBS, washed and re-suspended in

23 lysis buffer A (15 mM KCl, 10 mM Hepes, 2 mM $MgCl_2$, 0.1 mM EDTA, 1 mM phenylmethylsulfonyl

24 fluoride (PMSF), 1 mM DTT, 10 μg/mL aprotinin, 2 μg/mL leupeptin, 0.1% v/v NP-40, pH 7.6). This

suspension was incubated for 10 min on ice with occasional vortexing and centrifuged at 13,000 x g for

30 s to pellet nuclei. The supernatant (cytosolic fraction) was transferred into a new series of tubes.

Nuclei were rinsed with 0.2 mL of wash buffer B (2 M KCl, 25 mM HEPES, 0.1 mM EDTA, 1 mM

PMSF, 1 mM DTT, 10 μg/mL aprotinin, 2 μg/mL leupeptin, pH 7.6) and incubated at 4°C for 20 min.

Then an equal volume of buffer C (25 mM HEPES, 0.1 mM EDTA, 20% v/v glycerol, pH 7.6) was

added, the mix was centrifuged at 20,000 x g for 15 min and the supernatant (nuclear fraction) was

collected. The protein content was measured in both cytosolic and nuclear extracts; samples were

stored at -80°C until use. Doxorubicins content in the nuclear extracts was measured as described

above.

Cell cycle analysis. Cells were washed twice with fresh PBS, incubated in 0.5 mL ice-cold ethanol

70% v/v for 15 min, then centrifuged at 1,200 x g for 5 min at 4°C and rinsed with 0.3 mL of citrate

buffer (50 mM Na_2HPO_4, 25 mM sodium citrate, 1% v/v Triton X-100), containing 10 μg/mL

propidium iodide and 1 mg/mL RNAse (from bovine pancreas). After a 15 min incubation in the dark,

the intracellular fluorescence was detected by a FACSCalibur flow cytometer. For each analysis,

10,000 events were collected and analyzed by the Cell QuestPro software (Becton Dickinson).

Comet assay. The Single Cell Gel Electrophoresis assay (Comet assay), performed as reported

previously [23], was used to measure the doxorubicin-induced DNA damage, as index of genotoxicity.

Images were quantified by the CometScore software (TriTek Corp., Sumerduck, VA).

Mitochondria isolation. To isolate mitochondrial fractions, cells were washed twice in ice-cold PBS,

then lysed in 0.5 mL mitochondria lysis buffer (50 mM Tris, 100 mM KCl, 5 mN $MgCl_2$, 1.8 mM ATP,

1 mM EDTA, pH 7.2), supplemented with protease inhibitor cocktail III (Calbiochem), 1 mM PMSF

and 250 mM NaF. Samples were clarified by centrifuging at 650 x g for 3 min at 4°C; the supernatant

was collected and centrifuged at 13,000 x g for 5 min at 4°C. This supernatant (cytosolic extract) was

transferred to a new series of tubes, and stored at -80°C after protein quantification. The pellet

containing mitochondria was washed once with lysis buffer and re-suspended in 0.25 mL mitochondria

resuspension buffer (250 mM sucrose, 15 mM K_2HPO_4, 2 mM $MgCl_2$, 0.5 mM EDTA). A 50 μL

aliquot was sonicated and used for the measurement of protein content or Western blotting. To confirm

the presence of mitochondrial proteins in the extracts, 10 μg of each sonicated sample were subjected to

SDS-PAGE and probed with an anti-VDAC/porin antibody (data not shown). Doxorubicins content in

the mitochondrial extracts was measured as described above.

Reactive nitrogen species (RNS) and reactive oxygen species (ROS) measurement. RNS were

measured in the mitochondrial extracts by quantifying the amount of nitrotyrosines, an index of

peroxynitrite production, with the Nitrotyrosine ELISA kit (Hycult Biotechnolohgy, The Netherlands)

following the manufacturer's instructions. The absorbance was read with a Packard EL340 microplate

reader (Bio-Tek Instruments) and converted into pmol/mg mitochondrial proteins according to the

titration curve. To measure intramitochondrial ROS, 100 μg unsonicated mitochondria were re-

suspended in 0.5 mL PBS, incubated for 30 min at 37°C with 5 μM of the fluorescent probe 5-(and-6)-

chloromethyl-2',7'-dichlorodihydro-fluorescein diacetate-acetoxymethyl ester (DCFDA-AM),

centrifuged at 13,000 x g at 37°C and re-suspended in 0.5 mL PBS. The fluorescence of each sample,

considered an index of ROS levels, was read at 492 nm (λ excitation) and 517 nm (λ emission). The

results were expressed as nmoles/mg cell mitochondrial proteins.

Tricarboxylic acid cycle (TCA) measurement. The glucose flux through tricarboxylic acid (TCA)

cycle was measured by radiolabeling cells with 2 μCi/mL [6-^{14}C]-glucose (55 mCi/mmol;

PerkinElmer). Cell suspensions were incubated for 1 h in a closed experimental system to trap the

$^{14}CO_2$ developed from[^{14}C]-glucose, and the reaction was stopped by injecting 0.5 mL of 0.8 N $HClO_4$.

The amount of glucose transformed into CO_2 through the TCA cycle was calculated as described [24]

and expressed as pmoles CO_2/h/mg cell proteins.

Mitochondrial respiratory chain assays. Mitochondria were extracted as described above. The electron flux from Complex I to Complex III was measured on 10 μg of non-sonicated mitochondrial extracts, as previously reported [25]. Each sample was incubated in the absence or presence of the Complex I inhibitor rotenone (50 μM), to measure the ubiquinone-independent and the ubiquinone-dependent electron flux, respectively. The reaction was followed for 5 min, using a Packard EL340 microplate reader (Bio-Tek Instruments). Results were expressed as nmoles reduced cytochrome c/min/mg mitochondrial proteins.

ATP measurement. The amount of ATP was measured on 20 μg of mitochondrial extracts or on 100 μL of cell supernatants with the ATP Bioluminescent Assay Kit (FL-AA, Sigma Aldrich Co.), using a Synergy HT Multi-Mode Microplate Reader (Bio-Tek Instruments). ATP was quantified as arbitrary light units; data were converted into nmoles/mg mitochondrial proteins, using a calibration curve previously set.

Mitochondrial damage. 1×10^6 cells re-suspended in 0.5 mL PBS were incubated for 30 min at 37°C with the fluorescent probe JC-1 (2 μmol/L; Biotium Inc, Hayward, CA), then centrifuged at 13,000 x g for 5 min and re-suspended in 0.5 mL PBS. The fluorescence of each sample was read using a Synergy HT Multi-Mode Microplate Reader (Bio-Tek Instruments): the red fluorescence, index of polarized mitochondria, was detected at λ = 550 nm (excitation) and λ = 600 nm (emission); the green fluorescence, index of depolarized and damaged mitochondria, was detected at λ = 485 nm (excitation) and λ = 535 nm (emission). The fluorescence units were used to calculate the percentage of green-fluorescent mitochondria versus red-fluorescent mitochondria.

Caspase activity. Cells were lysed in 0.5 mL of caspase lysis buffer (20 mM HEPES/KOH, 10 mM KCl, 1.5 mM MgCl$_2$, 1 mM EGTA, 1 mM EDTA, 1 mM DTT, 1 mM PMSF, 10 μg/mL leupeptin, pH 7.5). 20 μg cell lysates were incubated for 1 h at 37°C with 20 μM of the fluorogenic substrate of caspase-9 Ac-Leu-Glu-His-Asp-7-amino-4-methylcoumarin (LEHD-AMC) or of caspase-3 Ac-Asp-

Glu-Val-Asp-7-amino-4-methylcoumarin (DEVD-AMC), in 0.25 mL caspase assay buffer (25 mM HEPES, 0.1 % w/v 3-[(3-cholamidopropyl)dimethylammonio]-1-propanesulfonate (CHAPS), 10% w/v sucrose, 10 mM DTT, 0.01% w/v egg albumin, pH 7.5). The reaction was stopped by adding 0.75 mL ice-cold 0.1% w/v trichloroacetic acid and the fluorescence of AMC fragment released by active caspases was read using a LS-5 spectrofluorimeter (PerkinElmer). Excitation and emission wavelengths were 380 nm and 460 nm, respectively. Fluorescence was converted in pmoles/μg cell proteins, using a calibration curve prepared previously with standard solutions of AMC.

***In vitro* metabolic stability of nitrooxy-doxorubicin in rat and human liver microsomes.** ND, dissolved in water, was incubated at 10 μM concentration in 100 mM PBS with either 0.48 mg/mL RLM or human HLM proteins, as previously reported [26]. The enzymatic reactions were initiated by addition of a NADPH-regenerating system (NADPH-GS) consisting of 2 mM β-NADPH, 10 mM glucose-6-phosphate (G6P), 0.4 U/mL glucose-6-phosphate dehydrogenase. Reactions were terminated at regular time intervals (overall range 0-60 min) by adding a double volume of acetonitrile. HPLC analysis was performed on Agilent 1100 Series liquid chromatography system (Agilent Technologies, Palo Alto, CA, USA) equipped with a LiChroCART® 250-4,6 (Merck Millipore, Vimodrone, Italy) and coupled with UV-VIS detector, set at λ=234 nm. Analysis was carried out using gradient elution of a binary solution: eluent A was acetonitrile, eluent B consisted of an aqueous solution of formic acid (0.1%). The analysis started at 0% A for 3 min, then rapidly increased up to 98% in 12 min and finally remaining at 98% A until 18 min. The analysis was performed at flow rate of 0.8 mL/min and injection volume was 20 μL. The intrinsic clearance (Cl_{int}) was calculated by the equation:

$$Cl_{int} = k(min-1) \times [V]/[P]$$

where k is the rate constant for the depletion of substrate, V is the volume of incubation in μL and P is the amount of microsomal proteins [27].

Inhibition of CYP-activity. RLM were incubated with the pentoxyresorufin (PTR; substrate of CYP2B), ethoxyresorufin (ETR; substrate of CYP1A), benzyloxyresorufin (BZR, substrate of CYP1A, 2B, 2C and 3A), p-nitrophenol (PNF, substrate of CYP2E1) and [3-[(3,4-difluorobenzyl)oxy]-5,5-dimethyl-4-[4-(methylsulfonyl)phenyl]furan-2(5H)-one] (DFB, substrate of CYP3A4) in presence of 10 µmol/L ND, as previously reported [26]. Reactions were started by adding NADPH-GS. To study the type of ND-induced inhibition, RLM were pre-incubated with 10 µM ND for 15 min, in presence or absence of NADPH, and after 15 min, substrates were added to assay mixture. The effect of ND on phase II metabolism (glucuronyl and sulphate- transferase) was studied by using rat liver "precison cut" slices and 7-ethoxycumarine as substrate, as previously reported [28]: liver slices were incubated in 750 µL RPMI medium containing 10 µM ND and 50 µM ethoxycumarine. After 4 h incubation the formation of 7-OH-cumarine, 7-O-glucuronyl– and 7-O-sulphate cumarine were measured fluorimetrically at λ excitation = 370 nm, λ emission = 455 nm.

Metabolism modelling. The MetaSite computational procedure (version 5.1.1, https://www.moldiscovery.com/software/metasite; Molecular Discovery Ltd, Hertfordshire, UK) was used to perform an *in silico* analysis aimed at identifying possible metabolites and CYP isoforms involved in ND metabolism [29].

***In vivo* tumor growth.** 1×10^5 TUBO cell suspension, mixed with 100 µL Matrigel, were injected subcutaneously in 6 weeks-old female BALB/c mice, housed (5 per cages) under 12 h light/dark cycle, with food and drinking provided *ad libitum*. The tumor growth was measured daily by caliper and was calculated according to the equation $(LxW^2)/2$, where L = tumor length; W = tumor width. In a first experimental setting, when the tumor reached the volume of 100 mm^3 (day 21), mice were randomly divided in the following groups (8 mice/group) and treated on days 3, 9, 15 after randomization as it follows: 1) ctrl group, treated with 0.1 mL saline solution intravenously (i.v.); 2) Dox group, treated with 5 mg/kg doxorubicin i.v.; 3) Caelyx® group, treated with 5 mg/kg Caelyx® i.v.; 4) ND group,

treated with 5 mg/kg of the compound i.v.; 5) liposome ND, treated with 5 mg/kg of the compound i.v.; 6) folate-targeted liposomal ND group, treated with 5 mg/kg of the compound i.v. Tumor volumes were monitored daily by caliper and animals were euthanized by injecting i.m. zolazepam (0.2 mL/kg) and xylazine (16 mg/kg) at day 21 after randomization. Tumors were excised and photographed. In a second experimental setting, mice were inoculated with 100 mm^3-TUBO cells, randomly divided 3 days after inoculation and treated as reported above on day 3, 9 and 15 after tumor inoculation. Tumor growth was monitored until day 54, then animals were sacrificed. In a third experimental setting, mice bearing a 100 mm^3-tumor were randomly divided and treated on days 3, 9, 15 after randomization with 0.1 mL saline solution i.v. or with 5 mg/kg of LNDF i.v. ("Drug ON" period). Animals were left untreated for 2 weeks ("Drug OFF period"), subjected to the same treatment (i.e. 5 mg/kg LNDF i.v., once a week for 3 weeks on days 30, 36, 42 after randomization; "Drug ON" period), left untreated for 2 weeks ("Drug OFF period") and sacrificed on day 54. Tumors were excised, digested by mechanical dissociation followed by 1 h incubation in complete culture medium containing 1 mg/mL collagenase and 0.2 mg/mL hyaluronidase, for 1 h at 37 °C, then centrifuged at 12,000 x g for 5 min, plated in fresh medium and used and used until passage 10-12 after plating. From mice of each experimental setting, tumors, heart, liver, kidneys and lungs were collected, fixed in 0.4% v/v paraformaldehyde for 18 h, washed with PBS and cut into 1 mm^3-pieces. Tissues were re-suspended into 1 mL ethanol/HCl 0.3 N, then homogenized for 30 s at 15 Hz, using a TissueLyser II device (Qiagen, Hilden, Germany). An aliquot of the homogenates was used to measure the tissue proteins; the remaining part was used to measure the content of doxorubicins by fluorimetric assays, as described above. The fluorescence of the corresponding tumors and organs of untreated animals ("ctrl" groups), considered as intrinsic auto-fluorescence, was subtracted from the fluorescence of each corresponding tumor/organs sample of treated mice. Animal care and experimental procedures were approved by the Bio-Ethical Committee of the Italian Ministry of Health (#122/2015-PR).

Hematochemical parameters. The hematochemical parameters LDH, aspartate aminotransferase (AST), alanine aminotransferase (ALT), alkaline phosphatase (AP), creatinine, CPK-MB were measured on the same blood samples collected immediately after mice sacrifice, using commercially available kits from Beckman Coulter Inc. (Miami, FL). c-Tnt was measured with the Elecsys STAT immunoassay (Roche Diagnostics, Indianapolis, IN).

Immunoistochemistry analysis. Tumors and hearts were fixed in 4% v/v paraformaldehyde. The paraffin sections were stained with hematoxylin/eosin. Tumor sections were immunostained for Ki67 (Millipore, Billerica, CA), an index of cell proliferation, followed by a peroxidase-conjugated secondary antibody (1:100, Dako, Glostrup, Denmark), or stained with the *In Situ* Cell Death Detection Kit (Sigma Chemicals Co.), based on dUTP Nick End Labeling (TUNEL) staining as an index of intratumor apoptosis. Heart sections were stained with picrosirius red solution to detect fibrosis [30], with wheat germ agglutinin-Alexa Fluor™ 488 conjugate (Molecular Probes, Eugene, OR) as index of cell dimension. To detect inflammatory cells, permeabilized heart sections were treated with 0.3% H_2O_2 for 10 min to block endogenous peroxidases and with citric buffer for 10 min to unmask the antigen. After saturation, sections were immunostained with an anti-CD18 antibody (BMA Biomedicals, Augst, Switzerland), followed by a biotinylated anti-rat secondary antibody. Sections were finally incubated with 3,3'-diaminobenzideine (DAB) solution for 5 minutes and counterstained with hematoxylin, and examined with a Leica DC100 microscope and/or Leica Olympus provis AX70 (Leica Microsystems GmbH, Wetzlar, Germany; 10 x ocular lens, 20-40-60-100 x objective, depending on the assay). At least 5 microscope fields were analyzed for each condition.

Statistical Analysis. All data in the text and figures are provided as means$\pm$SD. The results were analyzed by a one-way analysis of variance (ANOVA) and Tukey's test, using Statistical Package for Social Science (SPSS) software (IBM SPSS Statistics v.19). $p < 0.05$ was considered significant.

1

Results

Preparation and characterization of folate-targeted liposomal nitrooxy-doxorubicin

To prepare folate-decorated liposomal nitrooxy-doxorubicin (LNDF) two different approaches were used and compared with respect to their technological features and *in vitro* effects. FA-PEG-DSPE conjugate was associated to liposomes either by addition during the preparation of the lipid film (LNDFm, resulting in the random orientation of folate on the external surface and into the aqueous core of liposomes) or by post insertion method by which the conjugate is micellized and incubated with pre-formed liposomes (LNDFpi, all targeting ligands are on the external leaflet of the liposomes).

The physicochemical characteristics of the different formulations are summarized in **Table 1**.

Liposomes displayed a dimensional range from about 180 nm to 205 nm and the particle size tended to increase in the folate-decorated formulations. All formulations showed a low polydispersity index, below 0.15, indicating a narrow and homogenous size distribution. Liposomes showed a negative zeta potential value that was lower for decorated liposomes compared to plain ones, due to the presence of folate negatively charged carboxylic group. In particular, the negative charge slightly decreased in the formulations prepared by post insertion method suggesting a higher amount of folate on liposomes surface. On the other hand, a strong decrease in the amount of ND encapsulated was observed in LNDFpi, indicating a release of ND from liposomes during the post insertion process. The amount of folate on the liposome surface was determined spectrophotometrically; as shown in **Table 2** the amount of ligand was higher on liposomes prepared by post insertion method as already observed for other formulations [31].

After 4 weeks of storage in HEPES buffer at 4 °C no appreciable liposomes size and/or zeta potential changes were detected for all formulations and no liposomes aggregation or precipitation was observed.

After dilution with HEPES buffer or FCS, liposomes did not show aggregation, even after 48 h at 37 °C and only in FCS an increase of the mean diameter was observed (up to about 400 nm).

ND leakage from liposomes was evaluated in FCS and HEPES buffer at 37°C: the release profile of ND from folate-targeted liposomes was quite similar to that observed for previously tested untargeted ones [13] (50% of the compound was released after 24 h in buffer and after 16 h in serum).

Folate-targeted liposomal nitrooxy-doxorubicin is highly retained and cytotoxic in Dox-resistant breast cancer cells

After a preliminary screening of the expression of folate receptor, Pgp and MRP1 in not-transformed epithelial breast MCF10A cells and in a panel of human and murine breast cancer cell lines (**Supplementary Figure 1A**), we selected human MCF7 cells, which had undetectable Pgp and MRP1 and very low expression of FAR on cell surface [32], human triple-negative MDA-MB-231 and murine TUBO cells, which had both high expression of Pgp and MRP1 (**Supplementary Figure 1A**) and surface FAR (**Supplementary Figure 1B**).

In time-course experiments, all the liposomal formulations containing ND were significantly more retained than free Dox and ND in Pgp-/FAR-negative MCF7 cells, without - as expected because of the absence of FAR - significant differences between formulations with or without FA (**Figure 1A**). By contrast, in both MDA-MB-231 and TUBO cells, the rank of intracellular doxorubicins retention followed this order: LNDF > LND > ND > Dox (**Figure 1A**). LNDFpi were slightly more accumulated than LNFDm (**Figure 1A**), likely as a consequence of the higher amount of FA present on liposome surface. LNDFm and LNDFpi were less slightly accumulated at 1-3 h in TUBO cells compared to MDA-MB-231 cells, but no significant differences were detected at later time points (**Figure 1A**). For both formulation types, the liposome uptake was FAR-specific, as suggested by competition assays (**Supplementary Figure 2**). In all cell lines the amount of Dox and ND gradually decreased at 48 or 72 h compared to 24 h. By contrast, the amount of Dox in cells treated with LND or LNDF, was stable at

48 and 72 h, either in Pgp-negative MCF7 cells or in Pgp-positive MDA-MB-231 and TUBO cells **(Figure 1A).**

In MCF7 cells, but not in MDA-MB-231 and TUBO cells, Dox increased nitrite release (**Figure 1B**). In all cell lines, free ND or LND increased nitrite levels more than Dox. In the FAR-positive MDA-MB-231 and TUBO cells, LNDF produced the highest release of nitrite (**Figure 1B**), in line with the higher compound uptake in these cells.

Higher are the intracellular retention of doxorubicines and the increase of NO, higher is the cytotoxicity [8,11,13]. Consistently, the acute cytotoxicity, measured by the extracellular release of LDH (**Figure 1C**) and the reduction on cell survival, measured by the neutral red staining (**Figure 1D**), followed the trend of compound accumulation and nitrite levels.

LNDF formulations were not more accumulated than free Dox, ND or LND in FAR-negative/Pgp-negative not-transformed breast epithelial MCF10A cells (**Supplementary Figure 3A**), they did not increase the release of LDH (**Supplementary Figure 3B**) nor reduced cell viability more than Dox (**Supplementary Figure 3C**). Overall, LNDF induced less cytotoxicity in MCF10A cells than in MCF7 breast cancer cells (**Figure 1**).

The anti-tumor observed effects were not tumor-type specific: indeed, in human osteosarcoma U-2OS cells, which had high expression of FAR (**Supplementary Figure 4A**), LNDF was accumulated (**Supplementary Figure 4B-C**), increased nitrite (**Supplementary Figure 4D)** and LDH release (**Supplementary Figure 4E**), decreased cell viability (**Supplementary Figure 4F**) more than Dox, ND or LND. Starting from these data, we are currently expanding the investigation on the efficacy of LNDF on different Pgp-/FAR-positive tumors.

Folate-targeted liposomal nitrooxy-doxorubicin induces cell death with mitochondria- and nuclei- dependent mechanisms

As previously observed, Dox has a typical nuclear localization, whereas ND – either as free drug or liposomal formulation – had a peculiar mitochondrial accumulation [13]. Dox had low intranuclear (**Figure 2A, 2B**) and intramitochondrial (**Figure 2C, 2D)** in MDA-MB-231 cells, in consequence of its poor intracellular accumulation (**Figure 1A**). ND and LND LNDF displayed low intranuclear localization (**Figure 2A, 2B**) and relevant intramitochondrial localization (**Figure 2C, D**). Curiously, LNDF delivered drug to both nuclei and mitochondria (**Figure 2A-D**). The fluorescence and confocal microscope findings were confirmed by the HPLC quantification of compounds in nuclear and mitochondria extracts (**Supplementary Figure 5**).

Dox elicits antitumor effects by inhibiting topoisomerase II activity, inducing cell cycle arrest and DNA damage, and by several other mechanisms, including the impairment of mitochondrial energy metabolism and the generation of ROS *via* the mitochondrial electron transport chain [33]. We thus investigated the mechanisms at the basis of higher cytotoxic efficacy of LNDF, hypothesizing that both nucleus- and mitochondria-dependent mechanisms can be involved.

Dox did not induce cell cycle arrest in drug resistant MDA-MB-231 cells (**Figure 3A**) or genotoxic effects, evaluated by COMET assay (**Figure 3B; Supplementary Figure 6**). Also ND and LND did not alter the cell cycle distribution, except for an increase of sub-Go cells, suggestive of apoptotic cells (**Figure 3A**) and did not produce significant DNA damages (**Figure 3B; Supplementary Figure 6**). Although both ND and LND were cytotoxic also in drug resistant cells (**Figure 1C-D**), their prevalent mitochondrial localization likely prevented the toxicity dependent on nuclear mechanisms. By contrast, the higher nuclear delivery of LNDF made the drug able to exert nuclear toxicity, as demonstrated by the wide alteration of cell cycle distribution (i.e. the increased percentage of sub-Go cells and of cells arrested in G2/M phase, **Figure 3A**) and by the significant genotoxicity (**Figure 3B; Supplementary Figure 6**).

Dox did not exert any mitochondrial-dependent cytotoxicity in resistant MDA-MB-231 cells; e.g. it did not increase intra-mitochondrial reactive nitrogen species RNS (**Figure 3C**) and ROS (**Figure 3D**), it did not impair tricarboxylic acid (TCA) cycle (**Figure 3E**), electron transport (**Figure 3F**), ATP levels (**Figure 3G**) and mitochondrial membrane potential (**Figure 3H**), and it did not activate caspase 9 (**Figure 3I**) and caspase 3 (**Figure 3J**). By contrast, ND - as free drug, LND or LNDF - increased intra-mitochondrial RNS and ROS, decreased TCA cycle, electron flux and ATP amounts, induced mitochondrial depolarization and caspase 9/3 activation (**Figure 3C-J**), likely in consequence of the high intra-mitochondrial accumulation of ND achieved with all these formulations (**Figure 2B and 2D**).

Nitrooxy-doxorubicin is metabolically stable

The metabolic stability of ND was assessed in rat liver microsomes (RLM) and human liver microsomes (HLM). The cytochrome P450 (CYP)-dependent metabolism of ND followed a classic first order decay kinetic. The calculated intrinsic clearance (Cl_{int}) values were similar in both preparations (**Supplementary Table 1**) and suggested a high metabolic stability [27]. ND did not change the depletion rate of substrates of most rat CYP isoforms (data not shown), with the exception of 3-[(3,4-difluorobenzyl)oxy]-5,5-dimethyl-4-[4-(methylsulfonyl)phenyl]furan-2(5H)-one (DFB), a substrate of CYP3A4. In this case, the formation rate of the product (3-hydroxy-5,5-dimethyl-4-[4-(methylsulfonyl)phenyl]furan-2(5H)-one, DFH) was inhibited in a competitive manner by 15% and 20% after 15 and 30 min incubation time, respectively (**Supplementary Figure 7A**). Since DFB is O-dealkylated to DFH to a similar extent by rat CYP3A2 and human CYP3A4 isoforms [34], this result suggests that CYP3A isoform is the main isoenzyme involved in ND metabolism in both mammalian species. These data were supported by the *in silico* prediction of ND metabolites (Metasite software), that confirmed that CYP3A is the main isoform involved in the human metabolism of ND (with a

1   minor contribution of CYP2D6 and CYP2C19) and indicated that the O-demethylate derivative is the

2   most probable metabolite.

3   Phase II metabolism was minimally affected by ND: although ND reduced the formation of phase I

4   metabolite 7-OH cumarine (-15%) and of phase II sulphate metabolite (-25%), such decrease was not

5   statistically significant. Also the amount of glucuronide products did not differ in the absence or in the

6   presence of ND (**Supplementary Figure 7B**). The latter results, obtained in "precision-cut" rat liver

7   slices, an *in vitro* model closely resembling the *in vivo* conditions, allow us to hypothesize that ND can

8   affect the *in vivo* CYP activities at lower extent than the parent compound Dox [35].

9   **Folate-targeted liposomal nitrooxy-doxorubicin is effective against Pgp-positive tumors *in vivo***

10   On the basis of the promising results obtained by LNDF *in vitro* and the good metabolic profile of ND,

11   we next validated the efficacy of LNDF in the pre-clinical model of Pgp-/FAR-positive cells,

12   implanting a lethal amount of TUBO cells in syngeneic female BALB/c mice [36] (**Figure 4A**). Since

13   the liposomes prepared by adding folate in the phospholipids mixture (LNDFm) or by post insertion

14   (LNDFpi) technique gave superimposable results in all the assays *in vitro*, we only used the former

15   formulation - that was characterized by higher amount of encapsulated ND - for the *in vivo* experiments

16   (named as LNDF). Dox - as well as Caelyx[®] - did not reduced tumor growth (**Figure 4B-C**), whereas

17   the ND formulations were progressively more effective, following this rank order: ND < LND < LNDF

18   (**Figure 4B-C**). The reduced tumor growth was paralleled by a progressive decrease of tumor cell

19   proliferation, as revealed by Ki67 staining, and by a progressive increase of intratumor apoptotic areas,

20   as revealed by TUNEL staining (**Figure 4D**). This pattern replicates *in vivo* the main anti-proliferative

21   mechanisms exerted by LNDF *in vitro*. The growth of TUBO tumors is significantly reduced by 15

22   mg/Kg Dox or Caelyx[®] [37]. We achieved a significant reduction of tumor growth with a three-fold

23   lower dose of LNDF.

In addition, when administered for 3 weeks starting at early stages of tumor development, i.e. 3 days after tumor implants (**Figure 5A**), LNDF and – at lesser extent – ND and LND effectively retarded tumor growth, differently from free Dox or Caelyx® (**Figure 5B-C**).

In our experimental conditions, Dox did not alter cardiac tissue morphology, did not induce fibrosis, did not increase intracardiac infiltration of inflammatory cells and did not induce significant changes in cardiomyocyte cross sectional area (**Supplementary Figure 8**). LNDF did not alter these parameters as well (**Supplementary Figure 8**). The only signs of cardiac toxicity induced by Dox – in both experimental setting of Figure **4** and **5** – was the increase in cardiac troponin (c-Tnt; **Supplementary Tables 2-3**), as it usually occurs for a cumulative dose of Dox > 12 mg/kg [38]. As expected, Caelyx® prevented c-Tnt increase. Of note, LND and LNDF were similar to Caelyx®. Also, they did not induce liver or kidney toxicity, according to the hematochemical parameters (**Supplementary Tables 2-3**).

In line with the different reduction of tumor growth and the hematochemical parameters, in both experimental settings described above (**Figure 4-5**), ND, LND and LNDF were more retained than Dox and Caelyx® within the tumors, following this order: LNDF>LND>ND **(Supplementary Figure 9A-B)**. Dox was the drug mostly accumulated within heart, followed by ND. The intracardiac accumulation of LND and LNDF was similar to Caelyx® **(Supplementary Figure 9A-B)**. All liposomal formulations (Caelyx®, LND and LNDF) were more accumulated than free drugs (Dox and ND) in liver **(Supplementary Figure 9A-B)**, although such accumulation was apparently not associated to liver damage, as suggested by the lack in increase of transaminase, alkaline phosphatase and LDH **(Supplementary Tables 2-3)**. No significant differences were detected in the levels of free drugs and liposomal formulation in kidneys. Interestingly, Caelyx®, LND and LNDF resulted less accumulated than Dox or ND in lungs **(Supplementary Figure 9A-B).**

Dox dose-dependently increased the acute cardiotoxicity, inducing significant increase of creatine-phosphate kinase (CPK-MB) and c-Tnt at 12.5 mg/kg and 25 mg/kg dosages (**Supplementary Table**

4). Caelyx$^{®}$ and the liposomal formulations of ND did not elicit any acute increase of these parameters at each dosage tested (**Supplementary Table 4**), suggesting that liposomal formulations of ND had a cardiovascular safety profile superior to Dox and comparable to Caelyx$^{®}$.

Cells treated with folate-targeted liposomal nitrooxy-doxorubicin retain the same sensitivity of chemonaïve cells to the drug

To evaluate whether the response of tumors to LNDF was progressively reduced over the time, animals bearing a 100 mm^3-tumor were subjected to 2 cycles of treatment with LNDF (one LNDF administration/week for 3 consecutive weeks) followed by a 2-week drug-holiday period (**Figure 6A**). The rate of tumor growth remained low either after the first or the second cycle of treatment (**Figure 6B**), and the final tumor volume was significantly lower than the volume of animals receiving vehicle (**Figure 6C**). Also in this experimental setting, animals treated with repeated cycles of LNDF did not had signs of liver, kidney or heart toxicity (**Supplementary Table 5**). The amount of Dox in tumors and organs in animals treated with LNDF was lower in this experimental setting (**Supplementary Figure 9C**), where the animal sacrifice occurred 2 weeks after the last treatment than in the previous experimental settings, where the mice sacrifice occurred 1 week after the last LNDF administration (**Supplementary Figure 9A-B**).

Cells derived from treated tumors – re-plated and tested at passage 1, 5 (not shown) and 10-12 (**Figure 6D-F**) - were still resistant to Dox in terms of low drug accumulation (**Figure 6D**), low cytotoxicity (**Figure 6E**) and high cell viability (**Figure 6F**), but they retained the same sensitivity of chemonaïve cells (**Figure 1A, C-D**) to LNDF (**Figure 6D-F**).

Discussion

In this work we validated the efficacy of LNDF, a new FA-targeted liposomal formulation carrying a Dox-derivative designed to bypass the efflux mediated by Pgp, against breast cancer cells, where either

free Dox or Caelyx® were ineffective. The high expression of FAR is commonly observed in Dox-resistant cells of different histological origin [39]. Of note, comparing Dox-sensitive and Dox-resistant 4T1 breast cancer cells, FAR was significantly up-regulated in the latter [40], making FA-conjugated nanocarriers promising tools in increasing the drug delivery within resistant cells. By exploiting this feature, we validated the anticancer efficacy of LNDF in Pgp-highly expressing breast cancer cell lines (i.e MDA-MB-231 and TUBO cells) that showed a lower response to doxorubicin – in terms of drug-induced cytotoxicity *in vitro* – compared to Pgp-negative breast cancer MCF7 cells, and may be considered a good model of tumors constitutively resistant to Dox. LNDF uptake was lower in TUBO cells at 1-3 h, but it did not significantly differ between TUBO and MDA-MB-231 cells over the period 24-72 h, suggesting that our the delivery of doxorubicins induced by LNDF formulations granted a stable and durable drug delivery. This trend may be due to a lower endocytic rate of FAR in TUBO cells at short term, that may be compensated by an efficient FAR re-synthesis at long term that makes the expression of surface FAR equal in both the cell lines used.

Of note, in not-transformed breast epithelial MCF10A cells LNDF did not exert a cytotoxicity superior to Dox and was less toxic than in breast cancer cells with comparable undetectable levels of FAR and Pgp (such as MCF7 cells). This can be due to the low intracellular accumulation of LNDF and/or to the slow proliferation of MCF10A cells, a well-known feature that makes not-transformed cells more susceptible to DNA damaging agents like Dox than cancer cells. Since LNDF exerts its antitumor effects at significantly lower concentrations than Dox, we may reasonably suppose that it can be effective against Pgp-positive cancer cells at lower dosages than Dox, resulting less toxic than the latter on not-transformed breast epithelia.

Two types of FA-liposomes were prepared and compared. We observed that in LNDFm, in which the FA-PEG-DSPE conjugate was included in the lipid film prior to liposome formation, the targeting ligand amount on liposome surface was approximately the half of that of LNDFpi, in which the

conjugate was inserted by post insertion technique in preformed liposomes. However, LNDFpi showed a decrease in ND encapsulation efficiency; this can be due to a partial release of the compound from liposomes during the post insertion process that was done at a temperature near to the phase transition temperature of the lipid mixture, since ND is located in the hydrophobic region of the membrane bilayer, as we previously demonstrated [13]. The important reduction of drug content in liposomes was not observed in other works when Caelyx[®], in which Dox is encapsulated in the aqueous phase of liposomes, was decorated with FA using the same procedure [41]. However, the reduced amount of ND did not compromise the anti-tumor properties, since we did not detect any significant differences in the biological effects exerted by LNDFm and LNDFpi against Pgp-/FAR-positive cells. Thus, LNDFm was used for the further *in vivo* experiments.

It has been recently demonstrated that FA-targeted liposomes offer a significant advantage in the controlled delivery and intracellular activation of mitomycin-C prodrug in FAR-positive cells [42]. Similarly, the FA-decorated derivative of Caelyx[®] was more effective than Dox and Caelyx[®] against head and neck cancers over-expressing FAR [41]. However, the efficacy against Pgp-expressing cells was not tested. Our *in vitro* screening revealed that LNDF was accumulated in a FAR-dependent way, was more retained and more cytotoxic than free Dox or untargeted LND in Pgp-positive cells. In line with our data, FA-targeted pegylated liposomes loaded with paclitaxel exerted higher cytotoxicity against MDA-MB-231 cells than free paclitaxel or paclitaxel carried by untargeted liposomes [43]. Similarly, FA-targeted and pH-sensitive nanogels delivered Dox with high efficacy in Pgp-positive 4T1 breast cancer cells: this system allowed a significant reduction of Dox IC_{50} in resistant cells, independently on the presence of Pgp [40].

Paclitaxel and Dox are both Pgp substrate [1]. Taken together, these results suggest that the delivery through FA-targeted pegylated liposomes is a promising approach to increase the efficacy of chemotherapeutic drugs against FAR-positive and Pgp-positive cells. Since anthracyclines and taxanes

are first-line treatments in triple negative breast cancer [17], our work may provide the rationale for validating the efficacy of FA-targeted liposomal ND in this type of breast cancer.

Of note, the higher accumulation of LNDF was paralleled by the higher release of NO. We previously demonstrated that the nitration and subsequent inhibition of drug efflux transporters [11,13] triggers a "virtuous circle" that allows the increased retention of ND and toxicity. Moreover, we also demonstrated that the encapsulation of Dox into pegylated liposomes reduces Pgp activity: first, the phospholipids of the liposomal shell alter the plasma-membrane lipid environment where Pgp works [44]; second, pegylated distearoyl-phosphatidylethanolamine, a component of liposomal formulations, acts as an allosteric inhibitor of Pgp [45]. These inhibitory effects exerted by liposomal formulation on Pgp expression and activity [44-47] provide an additional benefit of LND and LNDF over free Dox of ND at long term. Indeed, while Dox and ND intracellular retention decreased 48 and 72 h after the exposure to the drug, likely reflecting the ND metabolism into Dox and further catabolites such as doxorubicinol [11] and/or the subsequent efflux of free Dox by Pgp, the amount of LND and LNDF remained stable. It is likely that FA-decoration, liposome encapsulation, pegylated phospholipids all contribute to the increase drug delivery and/or to the reduced efflux of ND form Pgp-/FAR-positive cells.

While Dox had a typical nuclear delivery and ND or LND had a typical mitochondrial localization [11,13], a peculiarity of LNDF was the delivery of its cargo to both nucleus and mitochondria. Mitochondrial delivery may be explained by the presence of ND, that has a strong tropism for mitochondria [11]. On the other hand, FAR has been detected in cytosol and nuclear compartments in ovary cancer biopsies [48]. It has been proposed that FAR localized on plasma-membrane follows an endosomal-lysosomal-mediated endocytic pathway, and that it migrated into the nucleus after the release from lysosomes [49]. Although we did not investigate the endocytic fate of FAR upon LNDF binding, the presence of intranuclear Dox in LNDF-treated cells supports this model. Dual ligand-

coupling strategies using liposomes decorated with FA and dexamethasone [50] have been successfully employed to increase the uptake of Dox and its nuclear delivery. Our formulation of LNDF, coupling the FAR-mediated uptake with the mitochondrial tropism of ND, offers the advantage of the simultaneous delivery of the chemotherapeutic drug to both nucleus and mitochondria. LNDF exerted cytotoxicity by nuclear-dependent mechanism, i.e. exerting classical pharmacodynamics effects of Dox [33], and mitochondrial-dependent mechanisms, i.e. reproducing the same effects of ND on mitochondria metabolism [11]. Triple negative breast cancers usually have multiple mechanisms of drug resistance, including ABC transporter overexpression, mutations in DNA repairing system enzymes, alterations in apoptosis [51]. Overcoming at the same time these multiple mechanisms of resistance is a challenging task in triple negative breast cancer treatment. Our results suggest that LNDF may be an effective tool to achieve this goal, since it combines the benefits derived from the active targeting and the benefits derived from the targeting of multiple pathways triggering cell death.

According to the latest guidelines, anthracycline-based monotherapy is one of the recommended treatment in the advanced stages of estrogen/progesterone receptor-negative breast tumors [52]. We then validated the efficacy of LNDF in preclinical models of estrogen/progesterone receptor-negative breast tumors, by inoculated a lethal amount of Pgp-/FAR-positive TUBO cells in syngeneic Balb/C mice [36]. This tumor model is characterized by fast grow, heavy infiltration of circulating inflammatory cells, in particular of M1-polarized macrophages that promote tumor growth and vascularization [53]. These features, suggestive of disorganized and highly fenestrated intra-tumor vasculature, favor the extravasation of liposomes as well. This hypothesis was supported by the high intra-tumor Dox still found in tumors 1 week after the last administration, that was 7.8-fold than free Dox, 4.9-fold more than Caelyx®, 2-fold more than ND and 1.3-fold more than LND. Since the one-pass circulation time of blood in mice is around 15 s [54], that is much shorter than the release time of ND from LNDF. Consistently, LNDF achieved greater therapeutic benefits than the currently used

anthracycline-based regimens (i.e. Dox and Caelyx[®]) on already formed tumors, suggesting that this liposomal formulation effectively delivered Dox within tumor core.

Interestingly, LNDF also delayed tumor growth when administered during the early phases of tumor development. FA is avidly taken up by rapidly dividing cells where it is used to support the synthesis of purines and the reaction of thymidylate synthase. We hypothesize that this biochemical need induces the high uptake of LNDF into rapidly growing TUBO tumors, explaining its high efficacy in preventing tumor growth.

At lesser extent, also LND and ND reduced the growth of already formed tumors and delayed tumor formation: this property may be due to the anti-cancer properties of NO [55], coupled with the concomitant delivery of drug. In line with the higher intratumor accumulation of FA-targeted liposomes versus untargeted ones [56], LNDF resulted however more effective than LND.

Interestingly, LNDF-treated tumors subjected to a chemotherapy regimen that mimics the regimes followed by patients (i.e. treatment cycles followed by "drug holiday" period) did not acquire secondary resistance to the drug. Although we cannot exclude that resistance to LNDF may occur at later time-points, we hypothesize that - at least during the period of the study - the presence of NO-releasing group, which is at the same time a component of ND and a MDR-reversing tool, preserves the chemosensitivity to our formulation.

In all the experimental settings, the liposomal formulations of ND had a cardiovascular safety profile superior to Dox and comparable to Caelyx[®]. The *post-mortem* analysis of Dox content in tumors and organs indicated that LNDF had the highest tumor vs. healthy tissues ratio accumulation and that the residual amount of Dox found in liver, heart, kidneys and heart in mice treated with this formulation was likely too low to induce detectable organ toxicity. LND and ND granted a lower intra-tumor accumulation, but they had a safe profile in terms of systemic toxicity. As expected, Caelyx[®] had the lowest intra-cardiac accumulation; on the other hand, its low intra-tumor accumulation made it

ineffective in reducing tumor growth. The residual Dox found in tumors and organs of animals treated with LNDF 2 weeks after the last treatment was lower than the amount found 1 week after the last treatment, suggesting that LNDF granted an effective and progressive clearance of the drug. Overall, these data further enforce the possibility of a future use of LNDF in clinical settings. Since our priority was to achieve a significant reduction of tumor growth in a model highly refractory to free Dox and Caelyx[®], we focused on this aspect in the present work. We did not plan at first a pharmacokinetic study of LNDF, hence we cannot predict a half-life for LNDF. We will perform such experiments in next future including either healthy mice and mice bearing different tumor types, given the variability in pharmacokinetic behavior that different tumors may produce on the same receptor-targeted liposomal formulation [57]. This step is necessary for the further preclinical development of LNDF.

In conclusion, in this work, we synthesized and validated an innovative folate-targeted liposomal formulation effective against Pgp-positive/Dox-resistant tumors. The novelty of our formulation relies on the combination of: 1) a multi-target Dox-derivative that has been specifically conceived to inhibit Pgp-efflux and to induce cell death of drug-resistant cells by the simultaneous activation of independent pathways; 2) an active targeted liposomal formulation decorated with folate with the aim to increase the tumor selectivity and, consequently, improve the therapeutic outcome.

In preclinical models of Pgp-resistant breast tumors, our formulation has revealed superior efficacy to Dox and Caelyx[®], and a cardio-toxicological profile similar to Caelyx[®]. Over the last 20 years, Caelyx[®] has represented the greatest improvement in the field of anthracyclines, thanks to its reduced cardiotoxicity. On the other hand, Caelyx[®] has not demonstrated a superior anti-tumor efficacy than Dox in chemoresistant breast cancer patients [14]. Our formulation represents a step forward in improving the treatment of FAR-positive/Pgp-positive breast tumors.

Acknowledgements

Conflict of interest

The authors declare no conflict of interest.

References

[1] M.M. Gottesman, T. Fojo, S.E. Bates, Multidrug resistance in cancer: role of ATP-dependent transporters, Nat. Rev. Cancer 2 (2002) 48–58.

[2] A. Brózik, C. Hegedüs, Z. Erdei, T. Hegedus, C. Özvegy-Laczka, G. Szakács, B. Sarkadi, Tyrosine kinase inhibitors as modulators of ATP binding cassette multidrug transporters: substrates, chemosensitizers or inducers of acquired multidrug resistance?, Expert. Opin. Drug Metab. Toxicol. 7 (2011) 623–642.

[3] R. Callaghan, F. Luk, M. Bebawy, Inhibition of the multidrug resistance P-glycoprotein: time for a change of strategy?, Drug Metab. Dispos. 42 (2014) 623–631.

[4] G. Szakács, M.D. Hall, M.M. Gottesman, A. Boumendjel, R. Kachadourian, B.J. Day, H. Baubichon-Cortay, A. Di Pietro, Targeting the Achilles heel of multidrug-resistant cancer by exploiting the fitness cost of resistance, Chem. Rev. 114 (2014) 5753–5774.

[5] V. Tsouris, M.K. Joo, S.H. Kim, I.C. Kwon, Y.Y. Won, Nano carriers that enable co-delivery of chemotherapy and RNAi agents for treatment of drug-resistant cancers, Biotechnol. Adv. 32 (2014) 1037–1050.

[6] S. Doublier, D.C. Belisario, M. Polimeni, L. Annaratone, C. Riganti, E. Allia, D. Ghigo, A. Bosia, A. Sapino, HIF-1 activation induces doxorubicin resistance in MCF7 3-D spheroids via P-glycoprotein expression: a potential model of the chemo-resistance of invasive micropapillary carcinoma of the breast, BMC Cancer 4 (2012) e4.

[7] J. Kopecka, I. Campia, A. Jacobs, A.P. Frei, D. Ghigo, B. Wollscheid, C. Riganti, Carbonic anhydrase XII is a new therapeutic target to overcome chemoresistance in cancer cells, Oncotarget 6 (2016) 6776–6793.

[8] C. Riganti, E. Miraglia, D. Viarisio, C. Costamagna, G. Pescarmona, D. Ghigo, A. Bosia, Nitric oxide reverts the resistance to doxorubicin in human colon cancer cells by inhibiting the drug efflux, Cancer Res. 65 (2005) 516–525.

[9] K. Chegaev, C. Riganti, L. Lazzarato, B. Rolando, S. Guglielmo, I. Campia, R. Fruttero, A Bosia, A. Gasco, Nitric oxide donor doxorubicins accumulate into doxorubicin-resistant human colon cancer cells inducing cytotoxicity, ACS Med. Chem. Lett. 4 (2011) 494–497.

[10] K. Chegaev, A. Fraix, E. Gazzano, G.E. Abd-Ellatef, M. Blangetti, B. Rolando, S. Conoci, C. Riganti, R. Fruttero, A. Gasco, S. Sortino, Light-regulated NO release as a novel strategy to overcome doxorubicin multidrug resistance, ACS Med. Chem. Lett. 8 (2017) 361–365.

[11] C. Riganti, B. Rolando, J. Kopecka, I Campia, K. Chegaev, L. Lazzarato, A. Federico, R. Fruttero, D. Ghigo, Mitochondrial-targeting nitrooxy-doxorubicin: a new approach to overcome drug resistance, Mol. Pharm. 10 (2013) 161–174.

[12] E. Gazzano, K. Chegaev, B. Rolando, M. Blangetti, L. Annaratone, D. Ghigo. R. Fruttero, C. Riganti, Overcoming multidrug resistance by targeting mitochondria with NO-donating doxorubicins, Bioorg. Med Chem. 24 (2016) 967–975.

[13] I. Pedrini, E. Gazzano, K. Chegaev, B. Rolando, A. Marengo, J. Kopecka, R. Fruttero, D. Ghigo, S. Arpicco, C. Riganti, Liposomal nitrooxy-doxorubicin: one step over Caelyx in drug-resistant human cancer cells, Mol. Pharm. 11 (2014) 3068–3079.

[14] A. Gabizon, Y. Patil, N.M. La-Beck, New insights and evolving role of Pegylated liposomal doxorubicin in cancer therapy, Drug Resist. Updat. 29 (2016) 90–106.

[15] A.K. Bakrania, B.C. Variya, S.S Patel, Novel targets for paclitaxel nano formulations: hopes and hypes in triple negative breast cancer, Pharmacol. Res. 111 (2016) 577–591.

[16] Y.G. Assaraf, C.P. Leamon, J.A. Reddy, The folate receptor as a rational therapeutic target for personalized cancer treatment, Drug Resist. Updat. 17 (2014) 89–95.

[17] N. Harbeck, M. Gnant, Breast cancer, Lancet 389 (2017) 1134–1150.

[18] B. Székely, A.L. Silber, L. Pusztai, New therapeutic strategies for triple-negative breast cancer, Oncology (Williston Park) 31 (2017) 130–137.

[19] T.M. Allen, P. Sapra, E. Moase, Use of the post-insertion method for the formation of ligand-coupled liposomes, Cell Mol. Biol. Lett. 7 (2002) 217–219.

[20] G.R. Bartlett, Phosphorus assay in column chromatography, J. Biol. Chem. 234 (1959) 466−468.

[21] J.M. Saul, A. Annapragada, J.V. Natarajan, R.V. Bellamkondaa, Controlled targeting of liposomal doxorubicin via the folate receptor in vitro, J. Control. Release 92 (2003) 49–67.

[22] G. Gelsomino, P.A. Corsetto, I. Campia, G. Montorfano, J. Kopecka, B. Castella, E. Gazzano, D. Ghigo, A.M. Rizzo, C. Riganti, Omega 3 fatty acids chemosensitize multidrug resistant colon cancer cells by down-regulating cholesterol synthesis and altering detergent resistant membranes composition, Mol. Cancer. 12 (2013) e137.

[23] F.S. Freyria, B. Bonelli, M. Tomatis, M. Ghiazza, E. Gazzano, D. Ghigo, E. Garrone, B. Fubini, Hematite nanoparticles larger than 90 nm show no sign of toxicity in terms of lactate dehydrogenase release, nitric oxide generation, apoptosis, and comet assay in murine alveolar macrophages and human lung epithelial cells, Chem. Res. Toxicol. 25 (2012) 850–861.

[24] C. Riganti, E. Gazzano, M. Polimeni, C. Costamagna, A. Bosia, D. Ghigo, Diphenyleneiodonium inhibits the cell redox metabolism and induces oxidative stress, J. Biol. Chem. 279 (2004) 47726-47731.

[25] I. Campia, C. Lussiana, G. Pescarmona, D. Ghigo, A. Bosia, C. Riganti, Geranylgeraniol prevents the cytotoxic effects of mevastatin in THP-1 cells, without decreasing the beneficial effects on cholesterol synthesis, Br. J. Pharmacol. 158 (2009) 1777–1786.

[26] P. D'Elia, F. De Matteis, S. Dragoni, A. Shah, G. Sgaragli, M. Valoti, DP7, A novel dihydropyridine multidrug resistance reverter, shows only weak inhibitory activity on human CYP3A enzyme(s), Eur. J. Pharmacol. 614 (2009) 7–13.

[27] B. Williamson, C. Wilson, G. Dagnell, R.J. Riley, Harmonised high throughput microsomal stability assay, J. Pharmacol. Toxicol, Methods 84 (2017) 31–36.

[28] S. Dragoni, G. Franco, M. Regoli, M. Bracciali, V. Morandi, G. Sgaragli, E. Bertelli, M. Valoti, Gold nanoparticles uptake and cytotoxicity assessed on rat liver precision-cut slices, Toxicol. Sci. 128 (2012) 186–197.

[29] G. Cruciani, E. Carosati, B. De Boeck, K. Ethirajulu, C. Mackie, T. Howe, R. Vianello, MetaSite: understanding metabolism in human cytochromes from the perspective of the chemist, J. Med. Chem. 48 (2005) 6970–6979.

[30] M. De Acetis, A. Notte, F. Accornero, G. Selvetella, M. Brancaccio, C. Vecchione, M. Sbroggiò, M. Collino, D. Pacchioni, G. Lanfranchi, A. Aretini, R. Ferretti, A. Maffei, F. Altruda, L. Silengo, G.

Tarone, G. Lembo, Cardiac overexpression of melusin protects from dilated cardiomyopathy due to long-standing pressure overload, Circ. Res. 27 (2005) 1087–1094.

[31] D.L Iden, T.M. Allen, In vitro and in vivo comparison of immunoliposomes made by conventional coupling techniques with those made by a new post-insertion approach, Biochim. Biophys. Acta 1513 (2001) 207–216.

[32] H. Chen, R. Ahn, J. Van den Bossche, D.H. Thompson, T.V. O'Halloran, Folate-mediated intracellular drug delivery increases the anticancer efficacy of nanoparticulate formulation of arsenic trioxide, Mol. Cancer Ther. 8 (2009) 1955–1963.

[33] S. Granados-Principal, J.L. Quiles, C. L. Ramirez-Tortosa, P. Sanchez-Rovira, M.C. Ramirez-Tortosa, New advances in molecular mechanisms and the prevention of adriamycin toxicity by antioxidant nutrients, Food Chem. Toxicol. 48 (2010) 1425–1438.

[34] N. Chauret, N. Tremblay, R.L. Lackman, J.Y. Gauthier, J.M. Silva, J. Marois, J.A. Yergey, D.A. Nicoll-Griffith, Description of a 96-well plate assay to measure cytochrome P4503A inhibition in human liver microsomes using a selective fluorescent probe, Anal. Biochem. 276 (1999) 215–226.

[35] D.S Riddick, C. Lee, S. Ramji, E.C. Chinje, R.L. Cowen, K.J. Williams, A.V. Patterson, I.J. Stratford, C.S. Morrow, A.J. Townsend, Y. Jounaidi, C.S. Chen, T. Su, H. Lu, P.S. Schwartz, D.J. Waxman, Cancer chemotherapy and drug metabolism, Drug Metab. Dispos. 33 (2005) 1083–96.

[36] C. Riganti, H. Pinto, E. Bolli, D.C. Belisario, R.A. Calogero, A. Bosia, F. Cavallo, Atorvastatin modulates anti-proliferative and pro-proliferative signals in Her2/Neu-positive mammary cancer, Biochem. Pharmacol. 82 (2011) 1079–1089.

[37] J. Akhtari, S.M. Rezayat, M. Teymouri, S.H. Alavizadeh, F. Gheybi, A. Badiee, M.R. Jaafari, Targeting, bio distributive and tumor growth inhibiting characterization of anti-HER2 affibody coupling to liposomal doxorubicin using BALB/c mice bearing TUBO tumors, Int. J. Pharm. 505 (2016) 89–95.

[38] J.P. Bertinchant, A. Polge, J.M. Juan, M.C. Oliva-Lauraire, I. Giuliani, C. Marty-Double, J.Y. Burdy, P. Fabbro-Peray, M. Laprade, J.P. Bali, C. Granier, J.E. de la Coussaye, M. Dauzat, Evaluation of cardiac troponin I and T levels as markers of myocardial damage in doxorubicin-induced cardiomyopathy rats, and their relationship with echocardiographic and histological findings, Clin. Chim. Acta 320 (2003) 39–51.

[39] S.K. Sriraman, J. Pan, C. Sarisozen, E. Luther, V. Torchilin, Enhanced cytotoxicity of folic acid-targeted liposomes co-loaded with C6 ceramide and doxorubicin: in vitro evaluation on HeLa, A2780-ADR, and H69-AR cells, Mol. Pharm. 13 (2016) 428–437.

[40] Y. Chen, O. Tezcan, D. Li, N. Beztsinna, B. Lou, T. Etrych, K. Ulbrich, J.M. Metselaar, T. Lammers, W.E. Hennink WE, Overcoming multidrug resistance using folate receptor-targeted and pH-responsive polymeric nanogels containing covalently entrapped doxorubicin, Nanoscale. 9 (2017) 10404–10419.

[41] A. Scomparin, S. Salmaso, A. Eldar-Boock, D. Ben-Shushan, S. Ferber, G. Tiram, H. Shmeeda, N. Landa-Rouben, J. Leor, P. Caliceti, A. Gabizon, R. Satchi-Fainaro, A comparative study of folate receptor-targeted doxorubicin delivery systems: dosing regimens and therapeutic index, J. Control. Release 208 (2015) 106–120.

[42] Y. Patil, Y. Amitay, P. Ohana, H. Shmeeda, A. Gabizon, Targeting of Pegylated liposomal mitomycin-C prodrug to the folate receptor of cancer cells: intracellular activation and enhanced cytotoxicity, J. Control. Release 10 (2016) 87–95.

[43] M.V. Barbosa, L.O. Monteiro, G. Carneiro, A.R. Malagutti, J.M. Vilela, M.S. Andrade, M.C. Oliveira, A.D. Carvalho-Junior, E.A. Leite, Experimental design of a liposomal lipid system: a potential strategy for paclitaxel-based breast cancer treatment, Colloids Surf. B Biointerfaces 136 (2015) 553–561.

[44] C. Riganti, C. Voena, J. Kopecka, P.A. Corsetto, G. Montorfano, E. Enrico, C. Costamagna, A.M. Rizzo, D. Ghigo, A. Bosia, Liposome-encapsulated doxorubicin reverses drug resistance by inhibiting P-glycoprotein in human cancer cells, Mol. Pharm. 8 (2011) 683–700.

[45] J. Kopecka, G. Salzano, I. Campia, S. Lusa, D. Ghigo, G. De Rosa, C. Riganti, Insights in the chemical components of liposomes responsible for P-glycoprotein inhibition, Nanomedicine 10 (2014) 77–87.

[46] A.R. Thierry, A. Dritschilo, A. Rahman,. Effect of liposome on P-glycoprotein function in multidrug-resistant cells, Biochem. Biophys. Res. Commun. 187 (1992) 1098–1105.

[47] S. Zalipsky, M. Saad, R. Kiwan, E. Ber, N. Yui, T. Minko, Antitumor activity of new liposomal prodrug of mitomycin C in multidrug resistant solid tumors. Insights of the mechanism of action. J. Drug. Target. 15 (2007) 518–530.

[48] S. Markert, S. Lassmann, B. Gabriel, M. Klar, M. Werner, G. Gitsch, F. Kratz, A. Hasenburg, Alpha-folate receptor expression in epithelial ovarian carcinoma and non-neoplastic ovarian tissue, Anticancer Res. 28 (2008) 3567–3572.

[49] V. Boshnjaku, K.W. Shim, T. Tsurubuchi, S. Ichi, E.V. Szany, G. Xi, B. Mania-Farnell, D.G. McLone, T. Tomita, C.S. Mayanil, Nuclear localization of folate receptor alpha: a new role as a transcription factor, Sci. Rep. 2 (2012) e980.

[50] L. Xiong, X. Du, F. Kleitz, S.Z. Qiao, Cancer-cell-specific nuclear-targeted drug delivery by dual-ligand-modified mesoporous silica nanoparticles, Small 11 (2015) 5919–5926.

[51] E.A. O'Reilly, L. Gubbins, S. Sharma, R. Tully, M.H. Guang, K. Weiner-Gorzel, J. McCaffrey, M. Harrison, F. Furlong, M. Kell, A. McCann, The fate of chemoresistance in triple negative breast cancer (TNBC), BBA Clin. 3 (2015) 257–275.

[52] F. Cardoso, A. Costa, E. Senkus, M. Aapro, F. André, C.H. Barrios, J. Bergh, G. Bhattacharyya, L. Biganzoli, M.J. Cardoso, L. Carey, D. Corneliussen-James, G. Curigliano, V. Dieras, N. El Saghir, A.

Eniu, L. Fallowfield, D. Fenech, P. Francis, K. Gelmon, A. Gennari, N. Harbeck, C. Hudis, B. Kaufman, I. Krop, M. Mayer, H. Meijer, S. Mertz, S. Ohno, O. Pagani, E. Papadopoulos, F. Peccatori, F. Pernault-Llorca, M.J. Piccart, J.Y. Pierga, H. Rugo, L. Shockney, G. Sledge, S. Swain, C. Thomssen, A. Tutt, D. Vorobiof, B. Xu, L. Norton, E. Winer, 3rd ESO-ESMO international consensus guidelines for advanced breast cancer (ABC 3), Ann. Oncol. 28 (2017) 16–33.

[53] M. Coscia, E. Quaglino, M. Iezzi, C. Curcio, F. Pantaleoni, C. Riganti, I. Holen, H. Mönkkönen, M. Boccadoro, G. Forni, P. Musiani, A. Bosia, F. Cavallo, M. Massaia, Zoledronic acid repolarizes tumour-associated macrophages and inhibits mammary carcinogenesis by targeting the mevalonate pathway, J. Cell. Mol. Med. 14 (2010) 2803–2815.

[54] K. Welsher, S.P. Sherlock, H. Dai, Deep-tissue anatomical imaging of mice using carbon nanotube fluorophores in the second near-infrared window, Proc. Natl. Acad. Sci. USA. 108 (2011) 8943–8938.

[55] S. Huerta, S. Chilka, B. Bonavida, Nitric oxide donors: novel cancer therapeutics, Int. J. Oncol. 33 (2008) 909–927.

[56] S. Poh, V. Chelvam, P.S. Low, Comparison of nanoparticle penetration into solid tumors and sites of inflammation: studies using targeted and nontargeted liposomes, Nanomedicine (Lond) 10 (2015) 1439–1449.

[57] A. Gabizon, Targeted Drug Strategies for Cancer and Inflammation, Springer, 2011, pp. 217–247.

1 **Table 1**

2 Characteristics of liposomes containing nitrooxy-doxorubicin (means, *n*=3).

Formulation	Mean particle size (nm ± SD)	Polydispersity index	Zeta potential (mV ± SD)	Entrapment efficiency (%)*
LND	182 ± 5.1	0.119	-7.53 ± 0.6	90.6 ± 4.1
LNDFm	194 ± 4.0	0.148	-10.9 ± 0.5	95.2 ± 2.9
LNDFpi	205 ± 2.2	0.121	-13.6 ± 0.9	66.1 ± 3.2

3 *ratio between drug/lipid molar ratio after purification and drug/lipid molar ratio after extrusion.*

4

1 **Table 2**

2 Characteristics of folate-liposomes (means, *n*=3).

Formulation	Folate content (μM ± SD)	FA/L[a] (%)	Folate insertion efficiency[b] (%)	Average number of folate molecules inserted per liposome
LNDFm	18.1 ± 5.1	1.11 ± 0.21	30.7 ± 5.7	2820
LNDFpi	38.3 ± 5.4	2.43 ± 0.30	67.0 ± 7.7	5570

3 [a] *ratio between moles of folate on liposome surface and moles of lipids in the final liposomal*
4 *suspension*
5 [b] *ratio between moles of folate on liposome surface and moles of lipids in the final liposomal*
6 *suspension and the theoretical value*
7

Figure captions

Figure 1. Doxorubicins uptake in breast cancer cells

A. Pgp-/FAR-negative MCF7 cells, Pgp-/FAR-positive MDA-MB-231 and TUBO cells were incubated for 0, 1, 3, 6, 24, 48 and 72 h with 5 µM Dox (D), nitrooxy-doxorubicin (ND), liposomal nitrooxy-doxorubicin (LND), liposomal nitrooxy-doxorubicin decorated with folate added in the phospholipids mixture (LNDFm) or by post insertion (LNDFpi) technique. The intracellular amount of Dox was measured fluorimetrically in duplicate. Data are presented as means $\pm$ SD (n = 4). LNDFm/LNDFpi *vs* D: * p < 0.001; LNDFm/LNDFpi *vs* ND: ° p < 0.01; LNDFm/LNDFpi *vs* LND: [#] p < 0.001. **B.** Cells were grown as reported in **A** for 24 h. Nitrite levels in the cell supernatant, an index of NO amount, were measured spectrophotometrically in duplicate in the cell culture supernatant. Data are presented as means$\pm$SD (n = 4). *Vs* untreated (-) cells: * p < 0.001; ND/LND/LNDFm/LNDFpi *vs* D: ° p < 0.01; LNDFm/LNDFpi *vs* ND: [#] p < 0.001; LNDFm/LNDFpi *vs* LND: [§] p < 0.001. C. Cells were grown as reported in **A** for 24 h. The release of LDH in the cell culture supernatant, was measured spectrophotometrically in duplicate. Data are presented as means$\pm$SD (n = 4). *Vs* untreated (-) cells: * p < 0.001; ND/LND/LNDFm/LNDFpi *vs* D: ° p < 0.05; LNDFm/LNDFpi *vs* ND: [#] p < 0.002; LNDFm/LNDFpi *vs* LND: [§] p < 0.005. **D.** Cells were grown as reported in **A** for 72 h. Cell viability was measured in quadruplicate by neutral red staining method. Data are presented as percentage of viable cells towards untreated cells (n = 4). *Vs* untreated (-) cells: * p < 0.001; ND/LND/LNDFm/LNDFpi *vs* D: ° p < 0.002; LNDFm/LNDFpi *vs* ND: [#] p < 0.05; LNDFm/LNDFpi *vs* LND: [§] p < 0.01.

Figure 2. Intracellular distribution of folate-targeted liposomal nitrooxy-doxorubicin

A. Pgp-/FAR-positive MDA-MB-231 cells were incubated 6 h with 5 µM Dox (D), nitrooxy-doxorubicin (ND), liposomal nitrooxy-doxorubicin (LND), liposomal nitrooxy-doxorubicin decorated with folate added in the phospholipids mixture (LNDFm) or by post-insertion method (LNDFpi), fixed

1   and counterstained with DAPI, then analysed for the intracellular doxorubicins (Doxo) localization by

2   fluorescence microscopy. The micrographs are representative of three experiments with similar results.

3   Bars: 20 μm. **B.** Nuclear fluorescence quantification by ImageJ software. Fluorescence units in Dox-

4   treated cells were considered as 1. Results were means±SD of three independent experiments.

5   ND/LND/LNDFm/LNDFpi *vs* D: * $p < 0.001$; LNDFm/LNDFpi *vs* ND: ° $p < 0.001$; LNDFm/LNDFpi

6   *vs* LND: [#] $p < 0.001$. **C.** Cells were transfected with expression vectors encoding for the GFP-fused-

7   leader sequence of E1 α pyruvate dehydrogenase to label mitochondria (mito) for 18 h, then incubated

8   as reported in **A.** The intracellular Doxo localization by confocal microscopy. The micrographs are

9   representative of three experiments with similar results. Bars: 10 μm. **D.** Mitochondrial fluorescence

10   quantification by ImageJ software. Fluorescence units in Dox-treated cells were considered as 1.

11   Results were means±SD of three independent experiments. ND/LND/LNDFm/LNDFpi *vs* D: * $p <$

12   0.001.

13   **Figure 3. Nucleus- and mitochondria-dependent cytotoxic effects folate-targeted liposomal**

14   **nitrooxy-doxorubicin in resistant cells**

15   Pgp-/FAR-positive MDA-MB-231 cells were incubated 24 h in fresh medium (-) or in medium

16   containing 5 μM Dox (D), nitrooxy-doxorubicin (ND), liposomal nitrooxy-doxorubicin (LND),

17   liposomal nitrooxy-doxorubicin decorated with folate added in the phospholipids mixture (LNDFm) or

18   by post-insertion method (LNDFpi). In panel **A-B** gemcitabine (50 μM for 24 h, GEM) was used as

19   control of DNA damaging agent. **A.** The cell cycle distribution was measured by flow cytometry. Data

20   are presented as means±SD (n=3). *Vs* untreated (-) cells: * $p < 0.05$. **B.** DNA damage was assessed by

21   Comet assay. The microphotographs are representative of DNA comets obtained in 3 experiments with

22   similar results. Bars = 10 μm. **C-D.** Intramitochondrial RNS (panel **C**) were measured in duplicate by a

23   specific ELISA, intramitochondrial ROS (panel **D**) were measured in duplicate fluorimetrically. Data

24   are presented as means±SD (n=4). For both panels, *vs* untreated (-) cells: * $p < 0.01$;

1 ND/LND/LNDFm/LNDFpi *vs* D: ° p < 0.01. **E.** The glucose flux through TCA cycle was measured in

2 cells radiolabeled with [6-^{14}C]-glucose. Data are presented as means$\pm$SD (n=3). *Vs* untreated (-) cells: *

3 p < 0.01; ND/LND/LNDFm/LNDFpi *vs* D: ° p < 0.01. **F-G**. The electron flux between Complex I and

4 III (panel **F**) was measured spectrophotometrically in duplicate, the ATP amount (panel **G**) was

5 measured by a chemiluminescence-based assay in duplicate in isolated mitochondria. Data are

6 presented as means$\pm$SD (n=3). For both panels, *vs* untreated (-) cells: * p < 0.005;

7 ND/LND/LNDFm/LNDFpi *vs* D: ° p < 0.05. **H.** The mitochondrial membrane potential was assessed

8 by the JC-1 staining method in duplicate. The percentage of green versus red mitochondria was

9 considered an index of mitochondrial depolarization and permeability transition. Data are presented as

10 means$\pm$SD (n=3). *Vs* untreated (-) cells: * p < 0.001; ND/LND/LNDFm/LNDFpi *vs* D: ° p < 0.001. **I-J.**

11 The activity of caspase 9 (panel **I**) and 3 (panel **J**) was measured fluorimetrically in the cytosolic

12 extracts. Data are presented as means$\pm$SD (n=3). For both panels, *vs* untreated (-) cells: * p < 0.001;

13 ND/LND/LNDFm/LNDFpi *vs* D: ° p < 0.001.

14 **Figure 4. Anti-tumor effects against of folate-targeted liposomal nitrooxy-doxorubicin against**
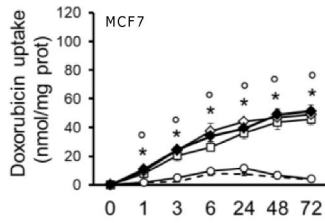
15 **resistant tumors**

16 Six weeks-old female BALB/c mice bearing a 100 mm^3-TUBO (i.e. Pgp-/FAR-positive) tumor were

17 randomly divided in the following groups (8 mice/group) and treated on days 3, 9, 15 after

18 randomization as it follows: 1) ctrl group, treated with 0.1 mL saline solution i.v.; 2) Dox (D) group,

19 treated with 5 mg/kg doxorubicin i.v.; 3) Caelyx$^®$ group, treated with 5 mg/kg Caelyx$^®$ i.v.; 4)

20 nitrooxy-doxorubicin (ND) group, treated with 5 mg/kg of the compound i.v.; 5) liposomal nitrooxy-

21 doxorubicin group (LND), treated with 5 mg/kg of the compound i.v.; 6) folate-targeted liposomal

22 nitrooxy-doxorubicin (LNDF) group, treated with 5 mg/kg of the compound i.v. Animals were

23 sacrificed at day 21 after randomization. **A.** Representative scheme of the treatment protocol. **B.** Tumor

24 growth monitored by caliper measurement. Data are presented as means$\pm$SD. ND/LND/LNDF *vs* ctrl

group: * $p < 0.01$; ND/LND/LNDF *vs* D: ° $p < 0.01$; LNDF *vs* ND: # $p < 0.001$; LNDF *vs* LND: § $p < 0.05$. **C.** Photographs of representative tumors from each treatment group after mice sacrifice. **D.** Sections of tumors from each group of mice were stained with hematoxylin and eosin (HE), immunostained with antibodies for Ki67 as an index of proliferation, or subjected to TUNEL staining as an index of apoptosis. Bar = 10 μm. The photograph is a representative of sections from five tumors.

Figure 5. Early administration of folate-targeted liposomal nitrooxy-doxorubicin retards the growth of Dox-resistant tumors

Six weeks-old female BALB/c mice were injected subcutaneously with 1 x 10 [5] Pgp-/FAR-positive-TUBO cells. At day 3 after injection, animals were randomly divided in the following groups (8 mice/group) and treated on days 3, 9, 15 after tumor inoculation as it follows: 1) ctrl group, treated with 0.1 mL saline solution i.v.; 2) Dox (D) group, treated with 5 mg/kg Dox i.v.; 3) Caelyx® group, treated with 5 mg/kg Caelyx® i.v.; 4) nitrooxy-doxorubicin (ND) group, treated with 5 mg/kg of the compound i.v.; 5) liposomal nitrooxy-doxorubicin group (LND), treated with 5 mg/kg of the compound i.v.; 6) folate-targeted liposomal nitrooxy-doxorubicin (LNDF) group, treated with 5 mg/kg of the compound i.v. Tumor growth was monitored until day 54, then animals were sacrificed. **A.** Representative scheme of the treatment protocol. **B.** Tumor growth was monitored by caliper measurement. Data are presented as means±SD. ND/LND/LNDF *vs* ctrl group (from day : * $p < 0.01$; ND/LND/LNDF *vs* D: ° $p < 0.01$; LNDF *vs* ND: # $p < 0.001$; LNDF *vs* LND: § $p < 0.05$. **C.** Photographs of representative tumors from each treatment group after mice sacrifice.

Figure 6. Doxorubicin-resistant tumors treated with folate-targeted liposomal nitrooxy-doxorubicin do not develop resistance after two cycles of treatment

Six weeks-old female BALB/c mice bearing a 100 mm^3-TUBO (i.e. Pgp-/FAR-positive) tumors were randomly divided in the following groups (10 mice/group) and treated on days 3, 9, 15 after randomization as it follows: 1) ctrl group, treated with 0.1 mL saline solution i.v.; 2) folate-targeted

liposomal nitrooxy-doxorubicin (LNDF) group, treated with 5 mg/kg of the compound i.v. ("Drug ON" period). Animals of ctrl group were sacrificed at day 24 after randomization for ethical reasons. Animals of LNDF group were left untreated for 2 weeks ("Drug OFF" period), subjected to the same treatment described above (i.e. 5 mg/kg LNDF i.v., once a week for 3 weeks on days 30, 36, 42 after randomization; "Drug ON" period), then left untreated for 2 weeks ("Drug OFF" period). Animals were sacrificed on day 54. Tumors from treated animals were excised, digested and re-plated for the *ex vivo* assays reported in panels **D-F. A.** Representative scheme of the treatment protocol. **B.** Tumor growth was monitored by caliper measurement. Data are presented as means±SD. For statistical analysis tumor volume of LNDF group until day 24 was compared with the tumor volume of the corresponding day in the ctrl group; tumor volume of LNDF group from day 27 to day 54 was compared with the tumor volume on day 24: * $p < 0.001$. **C.** Photographs of representative tumors from each treatment group after mice sacrifice. **D.** At passage 10-12 after re-plating, TUBO cells obtained from digested tumors of LNDF-treated animals were incubated for 6 h with 5 µM Dox (D) or LNDF. The intracellular amount of compounds was measured fluorimetrically in duplicate. Data are presented as means±SD (n=3). LNDF *vs* D: * $p < 0.001$. **E.** Cells were grown for 24 h in fresh medium (-) or in medium containing 5 µM Dox or LNDF. The release of LDH were measured spectrophotometrically in the cell culture supernatant in duplicate. Data are presented as means±SD (n=3). LNDF *vs* untreated (-) cells: * $p < 0.001$; LNDF *vs* D: ° $p < 0.001$. **F.** Cells were grown for 72 h as reported in **E.** Cell viability was measured in quadruplicate by neutral red staining method. Data are presented as percentage of viable cells towards untreated cells (n = 3). LNDF *vs* untreated (-) cells: * $p < 0.001$; LNDF *vs* D: ° $p < 0.001$.

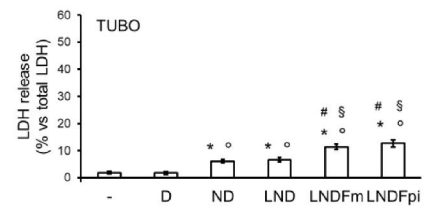# Figure 1

A Pgp/FAR negative cells   Pgp/FAR positive cells

B

C

D

1

2

Figure 2

A

	DAPI	Doxo	merge
D			
ND			
LND			
LNDFm			
LNDFpi			

C

	mito	Doxo	merge
D			
ND			
LND			
LNDFm			
LNDFpi			

B

Bar graph — Intranuclear doxo (RFU), y-axis 0–5; x-axis: D, ND, LND, LNDFm, LNDFpi. LNDFm and LNDFpi marked with °, #, *.

D

Bar graph — Intramitochondrial doxo (RFU), y-axis 0–5; x-axis: D, ND, LND, LNDFm, LNDFpi. ND, LND, LNDFm, LNDFpi marked with *.

1

2

Figure 3

Figure 4

A

Pgp$^+$/FR$^+$ TUBO cells

21 days

100 mm^3

sacrifice

B

Tumor volume (mm^3)

- ✳ ctrl
- ⊟ D
- ● Caelyx
- ■ ND
- △ LND
- ▲ LNDF

✳ #
○ §

day

C

ctrl   D   Caelyx

ND   LND   LNDF

D

	HE	Ki67$^+$ cells	Tunel$^+$ cells
ctrl			
D			
Caelyx			
ND			
LND			
LNDF			

1

2

Figure 5

Figure 6

A

Pgp⁺/FR⁺
TUBO cells

21 days → Drug ON → Drug OFF → Drug ON → Drug OFF → Cell replating

x 3   x 3

B

Tumor volume (mm³)

- ctrl
- LNDF

day

C

ctrl

LNDF

D

Intracellular doxorubicin (nmol/mg prot)

D   LNDF

E

LDH release (% vs total LDH)

ctrl   D   LNDF

F

Cell viability (% vs untreated cells)

ctrl   D   NDLF

1